J Mater Sci (2010) 45:3016–3022
DOI 10.1007/s10853-010-4304-z

Mechanical properties and morphology of microparticle and nanoparticle-filled polypropylene composites

Rui-Juan Zhou · Thomas Burkhart

Received: 30 September 2009 / Accepted: 6 February 2010 / Published online: 23 February 2010

Abstract Hydrophilic microparticle and nanoparticle-filled isotactic polypropylene (iPP) composites containing 5 wt% particles were extruded in a Berstorff extruder and then injection molded. For characterization the tensile and unnotched Charpy impact tests were performed. The results show that significant improvements in tensile strength, yield elongation, and unnotched impact strength are achieved in iPP/nanoparticle composite based on a good dispersion quality of nanoparticles. In the case of iPP/microparticle composite, the tensile modulus and yield strength are markedly increased compared to neat matrix, but the yield elongation and unnotched impact strength are drastically decreased due to broad size distribution of microparticles. The fracture mechanisms were discussed by studying surface morphology of failed samples. Furthermore, the influence of crystalline behavior on mechanical properties of iPP composites was discussed.

Introduction

In recent years, polymer-based composites have attracted increased attention in both industry and academia. Polymers can be modified with different fillers, which enhance the mechanical, thermal, and wear resistance properties of matrix. Polypropylene (PP), one of the most widely used plastics, has been the subject of intensive studies with the objective to improve its mechanical properties. Many studies have shown significant improvement in tensile and/or impact properties of PP composites filled with particles [1–7]. Chan et al. [8] have reported that the Izod impact strength of PP/$CaCO_3$ nanocomposites was drastically increased by approximately 300% and the notched impact toughness obtained by *J*-integral tests increased even by 500%. In the work of Thio et al. [9], the mechanical properties of PP composites containing $CaCO_3$ particles with average diameters of 0.07, 0.7, and 3.5 μm were evaluated. The authors found that the addition of 0.7 μm diameter particles improved Izod impact energy up to 4 times that of neat PP. The other particles used had either adverse or no effect on the impact toughness of PP. Huang et al. [10] have investigated the mechanical properties of nanosilica-filled PP composites. They found both the tensile strength and the notched impact toughness of PP composites were enhanced markedly after surface treatment of nanosilica. In addition, numerous studies revealed that the toughening and reinforcing effects of particles are strongly affected by many factors such as particle dispersion state, particle content and size, interfacial adhesion between matrix and fillers as well as test conditions, i.e., test speed, test temperature, annealing state, etc. [11–14].

The toughening of polymer plastics using inorganic particles has some rather complicated aspects, in which the crack front bowing mechanism has been treated as the major toughening mechanism in inorganic particle-filled thermosets. The crack bowing mechanism was first proposed by Lange [15]. According to this mechanism, the rigid particles in composites will resist the propagation of the crack. The initial primary crack has to bend between particles (bowing). The bowed secondary crack has more elastic energy stored than the straight unbowed crack. Therefore, more energy is needed for crack propagation in composites. This mechanism has successfully explained the toughening of polymers in many studies [16, 17].

R.-J. Zhou (✉) · T. Burkhart
Department of Materials Science, Institute for Composite Materials, Technical University of Kaiserslautern, Erwin-Schrödinger-Str, 67663 Kaiserslautern, Germany
e-mail: ruijuan.zhou@ivw.uni-kl.de

However, the applicability of this mechanism is questionable in the case where the rigid particles in the order of 50 nm or less, because such small particles may not be able to resist the propagation of the crack [8]. Lee et al. [18, 19] have developed a new mechanism to explain the toughening effect of particles based on glass bead-filled epoxies. They proposed three types of fracture processes, i.e., micro-shear banding, debonding of particles/shear yielding of matrix, and step formation, in which micro-shear banding is established as the major and most effective toughening mechanism. This mechanism is expected to give more detailed and fundamental understanding of inorganic particle toughening than the crack front bowing mechanism.

In general, one of the difficulties regarding the use of inorganic fillers in PP is the dispersion quality due to the hydrophobic nature of PP molecules, which gives a big problem in enhancing the adhesion between hydrophilic fillers and hydrophobic PP matrix. This problem can be overcome by addition of coupling agents such as maleic anhydride grafted PP, and by surface treatment of inorganic fillers or by in situ polymerization to create better bond strength between fillers and PP matrix. Traditional ways to prepare the composites include solution method, in situ polymerization, melt blending, template synthesis, and sol–gel technique, in which melt blending is favored in industry.

In this work, hydrophilic micro and nanoparticles were directly compounded into isotactic polypropylene (iPP) melt in an extruder, in which the screw was specially designed in order to achieve a good dispersion quality of micro and nanoparticles. Our goal of this work is to find the influence of micro and nanoparticles used on mechanical properties of iPP with comparable interfacial adhesion between matrix and particles. For that purpose, the dispersion quality of particles and the mechanical properties as well as the fracture morphology of iPP composites were examined.

Experimental

Materials and sample preparation

Granulated iPP homopolymer was purchased from LyondellBasell Polymers (Moplen-HP 400R). The melt flow rate and the density of this iPP are 25 g/10 min and 0.9 g/cm^3, respectively. The fumed nanosilica Aerosil 90 (A90) was provided from Evonik GmbH, Germany. The primary particle size of this nanosilica is 20 nm. The microparticle boehmite was friendly supplied by Sasol Germany under the trade name Dispal 60 (D60). The size distribution of particles measured in water is shown in Fig. 1. It can be seen that most particles are smaller than 1.0 μm.

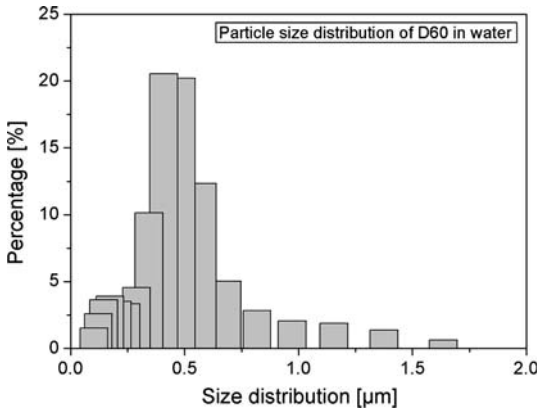

Fig. 1 Size distribution of microparticles measured in water

All raw materials were dried in an oven at 80 °C for 12 h. The iPP composites containing 5 wt% of micro and nanoparticles were prepared in a Berstorff co-rotating twin-screw extruder with a barrel temperature profile ranging from 180 °C near the hopper to 220 °C at the die. The screw speed was 150 rpm. The design of the screw configuration with a length-to-diameter ratio of 20 is given in Fig. 2. The shear forces by melt compounding are expected to be helpful to support the dispersion and deagglomeration of the respective particles. The iPP composites were extruded twice to ensure a better dispersion quality of particles. The palletized composite extrudates were then injection molded into specimens according to ISO standards for tensile test (ISO 527-1) and impact test (ISO 179).

Characterization

The static tensile test was performed using a Zwick 1474 universal testing machine according to DIN EN ISO 527-2-1B at room temperature. The crosshead speed was 4 mm/min. The tensile modulus, yield strength, and elongation at yield were determined. In order to determine the unnotched Charpy impact strength of samples (4 × 10 × 80 mm^3), impact test was performed using a pendulum test machine at 21 ± 1 °C. The weight of the pendulum hammer used was 1 kg and the test velocity at impact was 3 m/s. During the test, both the load and the deflection signals were recorded. In both mechanical tests, ten specimens for each material were tested and the average values were taken.

The crystallinity of matrix in neat iPP and iPP composites was determined by differential scanning calorimetry (DSC) using a Mettler Toledo instrument.

The morphology of iPP composites and the fracture surfaces of damaged samples were examined by using scanning electron microscopy (SEM, JEOL JSM-6300 and Hitachi S5200). The size distribution of microparticles in

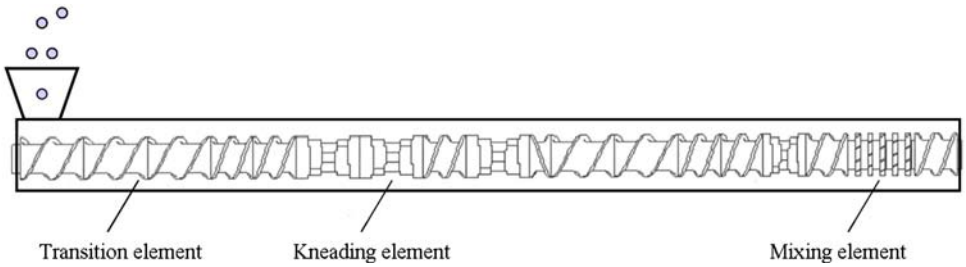

Fig. 2 Screw configuration of the co-rotating twin-screw extruder

iPP/D60 composite was analyzed by optical microscopy (Highlight 3000, Olympus Europe).

Results and discussion

Morphology of iPP composites

Figure 3 shows the morphology of iPP/D60 and iPP/A90 composites. It is seen that the microparticles D60 are relatively well dispersed in iPP matrix. According to SEM and optical microscopy analysis, 96.5% microparticles are distributed under 10 μm, 3.2% microparticles have the size in the range of 10–50 μm and only 0.3% particles are larger than 50 μm compared to in water, where the microparticles are 100% smaller than 2 μm, the size distribution in matrix becomes much broader indicating a high agglomeration degree. In iPP/A90 composite, the nanoparticles agglomerate slightly due to strong interaction between the particles, but most of them remain in a nanoscale range and homogenized in matrix. As seen in the figure, the adhesion between nanoparticles A90 and matrix is better than that between microparticles D60 and matrix; despite both particles have the similar hydrophilic surface nature. On the fracture surfaces of both composites, numerous small holes appear after particle debonding from the matrix indicating that the interaction between hydrophilic particles and hydrophobic polymer matrix is weak due to poor miscibility.

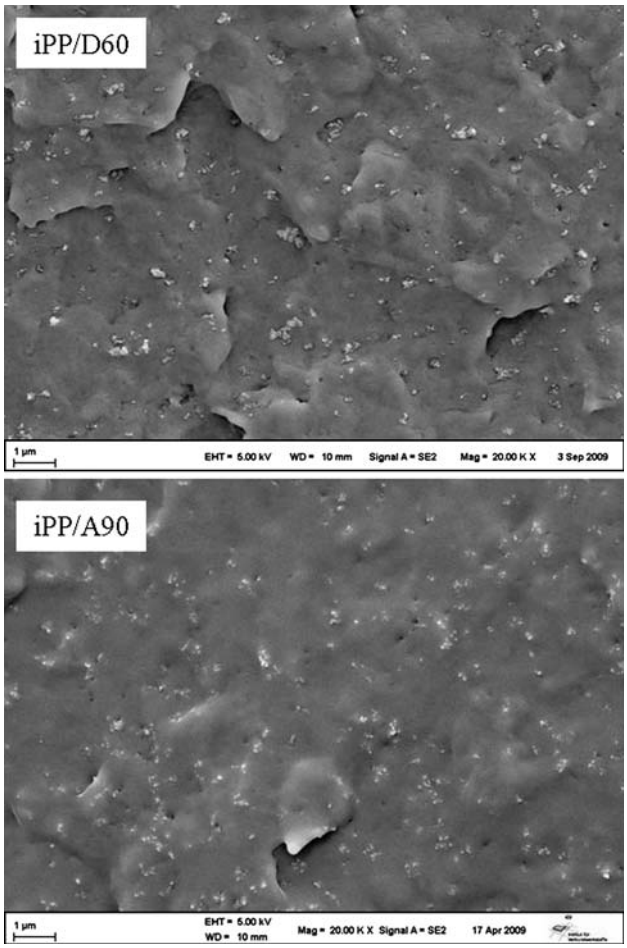

Fig. 3 SEM micrographs of iPP/D60 (5 wt%) and iPP/A90 (5 wt%) composites

Unnotched Charpy impact strength and fracture surface morphology

The impact force and energy as a function of displacement of samples are presented in Fig. 4a. After oscillation at initial stage, the impact force increases up to a maximum and then decreases to a value, at which the increasing impact energy attains its maximum. From this value the impact force drops steeply to zero and the impact energy keeps further constant. Figure 4a reveals that more energy is needed for a fracture process in iPP/A90 nanocomposite than in neat matrix, whereas the impact energy for iPP/D60 composite is clearly decreased compared to neat iPP. The unnotched Charpy impact strength, which was calculated as the energy consumed during the impact process per unit of fractured surface area, is presented in Fig. 4b. The unnotched Charpy impact strength of iPP/A90 nanocomposite is significantly improved by 14%. In contrast, the unnotched impact strength of iPP/D60 composite is drastically decreased by 30% in comparison with neat iPP. Regardless of particle types, the different effect of micro and nanoparticles on unnotched Charpy impact strength of iPP can be attributed to different size distribution of dispersed particles within matrix. The fracture morphology and mechanism will be discussed in detail.

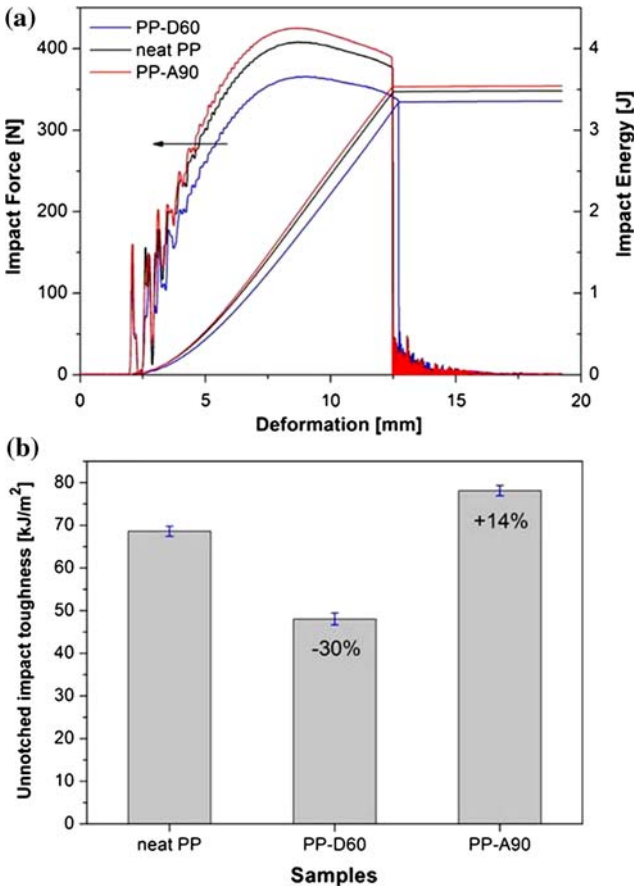

Fig. 4 (**a**) Impact force and energy as a function of sample deformation, (**b**) unnotched Charpy impact strength of materials tested

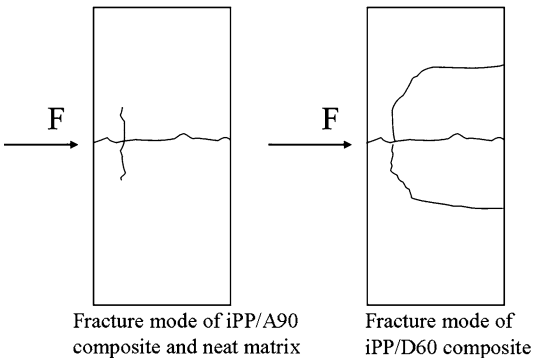

Fig. 5 Impact fracture modes of following samples: (**a**) neat iPP and iPP/A90 composite, (**b**) iPP/D60 composite

It is known that crazes or cracks in semicrystalline polymers such as iPP have a larger tendency to bifurcate or branch off compared with crazes in glassy polymers, because they propagate normally along the boundaries of the spherulites [20]. Macroscopically, all specimens tested in this work are damaged along the impact direction (primary crack) in a brittle fracture manner. Interestingly, the iPP/D60 specimens are completely damaged into four parts, whereas the specimens of iPP/A90 composite and neat matrix are not completely broken along the secondary crack which is vertical to the fracture surface, as shown in Fig. 5. This predicts different resistance to crack propagation in both composites.

SEM fractographs of fracture surfaces of failed specimens give much information on the impact fracture mechanisms and may explain the change of the unnotched impact strength of iPP matrix after addition of particles. Figure 6a and b shows the micrographs taken from fracture surfaces near the initial impact position of iPP/A90 nanocomposite and neat iPP matrix. The crack-propagation direction is indicated with a long white arrow in the graphs. It is evident that the analyzed region is divided into three subregions, namely the initial crack region A, the fracture process zone B, and the fast (unstable) crack-propagation zone C, as described in literature [11, 18]. According to Ref. [11], most energy is consumed in the stage A and B of fracture process while little energy is dissipated in the fast-crack-propagation stage C. From the figure, the length of subregion A in both micrographs is approximately 1 mm. In this region, shear banding (yielding) is the major mode of the plastic deformation of matrix. Away from the initial impact position, plastic deformation of matrix including shear banding and microcracks in iPP/A90 nanocomposite increases whereas it decreases in neat iPP. Besides plastic deformation, river-like bands perpendicular to the direction of crack propagation are also observed in zone B in iPP/A90 composite. These bands are formed where the crack fronts are arrested for a certain period of time and break away upon further loading. It is reported that the increasing amount of this crack-arrest band (or line) indicates an increased resistance to crack propagation [18]. Different from the iPP/A90 nanocomposite, the subregion B of neat matrix is much smoother and smaller. No significant plastic deformation is observed in this zone. The fracture surface morphology confirms that more extensive plastic deformation induced by nanoparticles took place in iPP/A90 samples than in neat iPP matrix during impact fracture process. The more plastic deformation of matrix, the more energy will be absorbed by impact test. This is the reason for the higher impact strength of iPP/A90 nanocomposite.

Figure 7 shows the micrographs of iPP/D60 fracture surfaces along the initial primary crack. Because the secondary crack propagates throughout the specimen, the three subregions A, B, and C on the fracture surface are located in different parts. The analyzed locations with respect to the broken impact specimen are indicated in the graphs. It can be seen that the subregion A is very small with a length of approximately 0.3 mm, indicating an earlier propagation of the primary crack. Slight plastic deformation of matrix is

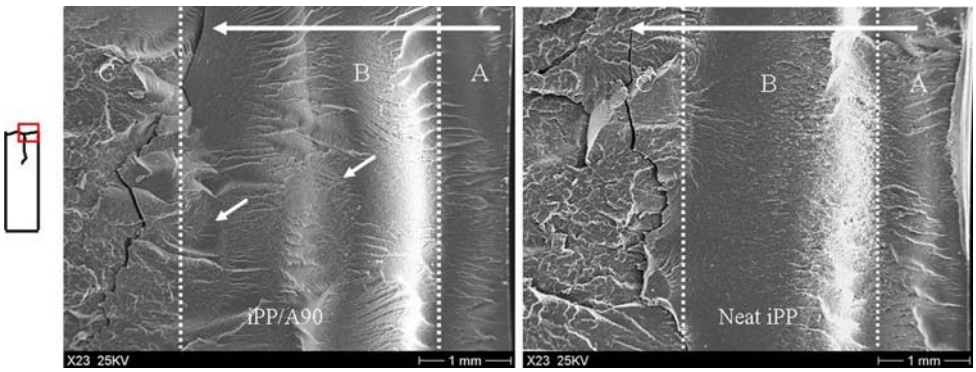

Fig. 6 SEM fractographs of impact fracture surfaces of neat iPP and iPP/A90 composite

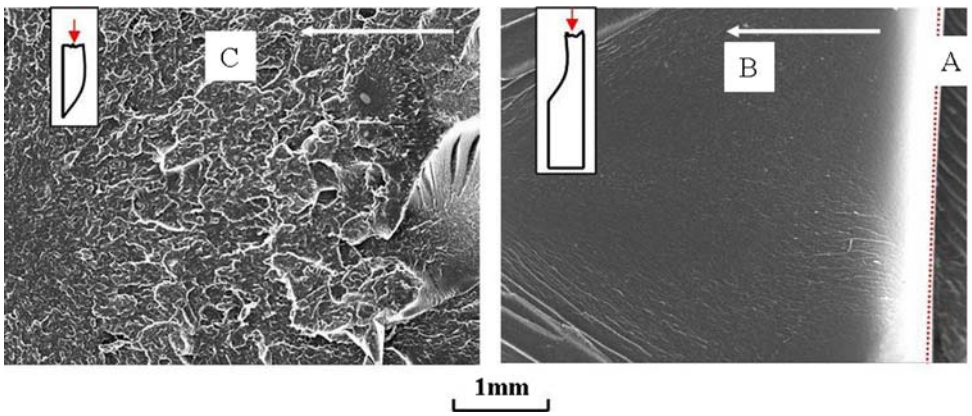

Fig. 7 SEM fractographs of impact fracture surfaces of iPP/D60 composite along the primary crack

observed in this region. Different from the subregions B in iPP/A90 and neat iPP samples, the subregion B in iPP/D60 is extremely smooth without any plastic deformation of matrix. This is an evidence of brittle fracture. The close-up views of fracture surfaces along the secondary crack are given in Fig. 8. Similar to subregion B, the fracture surfaces are very smooth on which some large agglomerates appear. Interestingly, typical features of crack-front bowing mechanism are observed around these agglomerates such as crack bowing, crack tearing, and particle debonding as indicated in figure. The step structures, which are known as characteristic tails in micro-shear banding mechanism [15], are formed behind particle agglomerates because of the mismatch between two planes of crack propagation which are divided by a particle (agglomerate). Despite of these energy-dissipating features occurring by impact test, the iPP/D60 composite shows decreased impact toughness by 30%. An explanation is that numerous micro voids were formed between matrix and large, stable agglomerates under impact loading due to poor matrix-agglomerate interaction. These voids grew and linked up, becoming sources of the secondary cracks and resulting in a profoundly deleterious effect on the impact toughness [21].

The fracture surface morphology reveals that the impact fracture is a combined result of crack bowing mechanism and micro-shear banding (yielding) mechanism, especially noticeable in the case of iPP/D60 composite. In the iPP/A90 nanocomposite, the micro-shear banding mechanism is more pronounced and gives more reasonable explanation for the toughening effect of nanoparticles.

Tensile properties and fracture surface morphology

The results of tensile test are presented in Fig. 9. The typical stress–strain curve in Fig. 9a shows that the iPP composites have higher yield strength and lower strain at break than neat matrix. This means the iPP matrix becomes less ductile after incorporation of particles. The important parameters obtained are shown in Fig. 9b–d. Compared to neat iPP matrix, the tensile modulus and yield strength of iPP/D60 composite are improved by 24 and 5%, respectively. The stiffening and strengthening effects of micro-particles can be attributed to formation of numerous cavitations (dimples) and cavitation-induced massive shear deformation of matrix as shown in Fig. 10. It is believed that the formation of these cavitations in composites is accompanied by energy dissipation, such as localized micro-deformation of matrix and particle debonding [22]. In the center of such cavitations, large particle agglomerates are found, which can act as stress concentrators in iPP matrix under tensile loading [23]. On the other hand, the

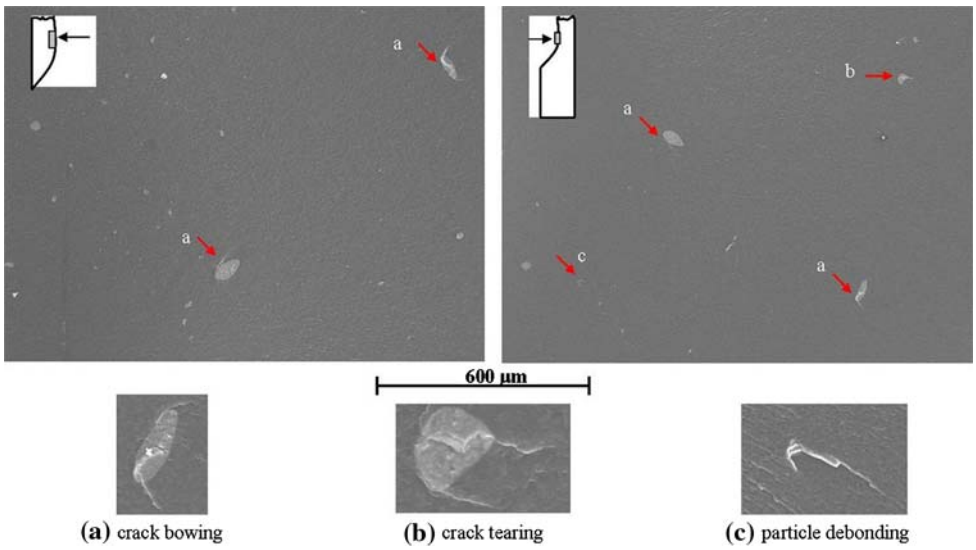

Fig. 8 SEM micrographs of fracture surfaces of iPP/D60 composite along the secondary vertical crack

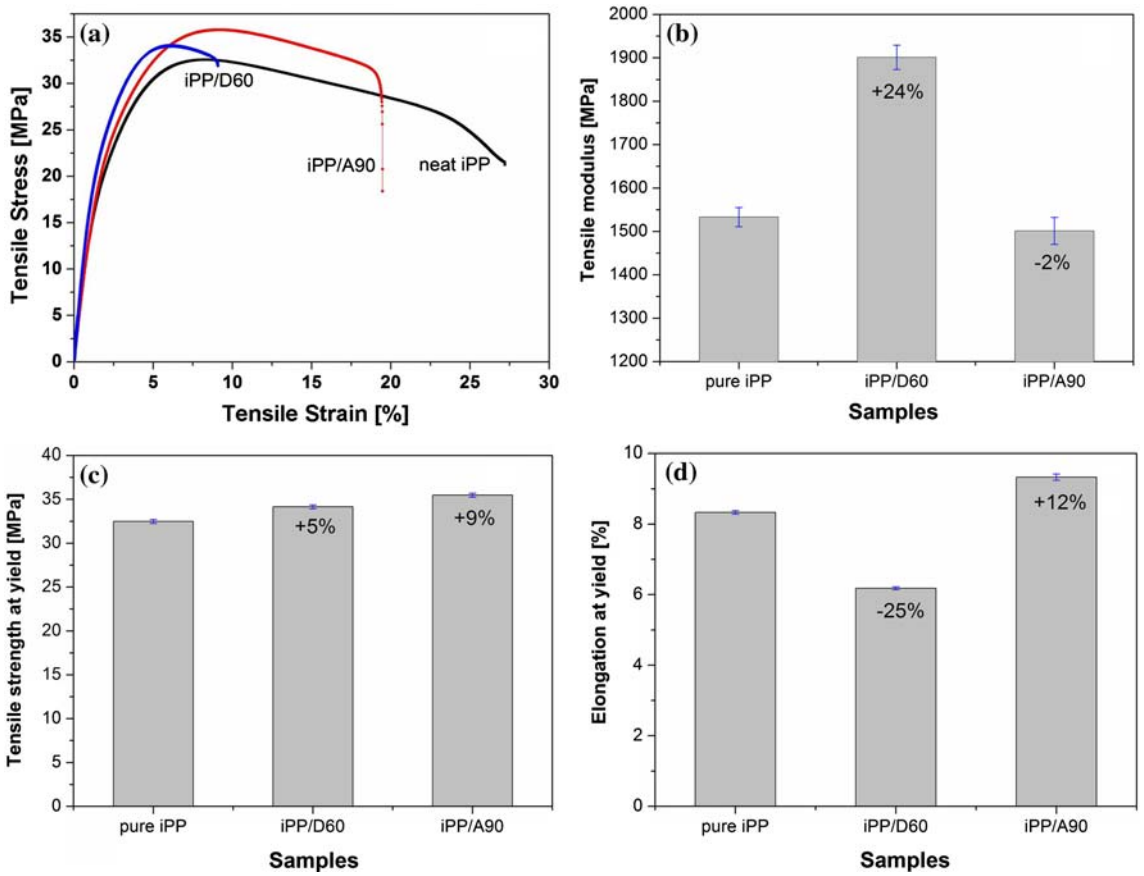

Fig. 9 Tensile test results of neat iPP, iPP/D60, and iPP/A90 composites: (**a**) stress-strain curves of all three samples, (**b**) tensile modulus, (**c**) tensile strength at yield, and (**d**) elongation at yield

presence of large agglomerates causes premature failure of matrix when an external force is imposed on the composite. As a result, the yield elongation decreases by 25% in comparison with neat iPP and the samples damaged much earlier during tensile test. In the case of iPP/A90 nanocomposite, improvements in both yield strength and yield elongation are achieved by 9 and 12%, respectively. The reasons are as follows: firstly, the cavitations induced by nanoparticles are much smaller, and their density increases obviously (Fig. 10). Therefore, more energy was stored by tensile test according to [22]. Secondly, the homogenized nanoparticles are too small to cause premature failure in

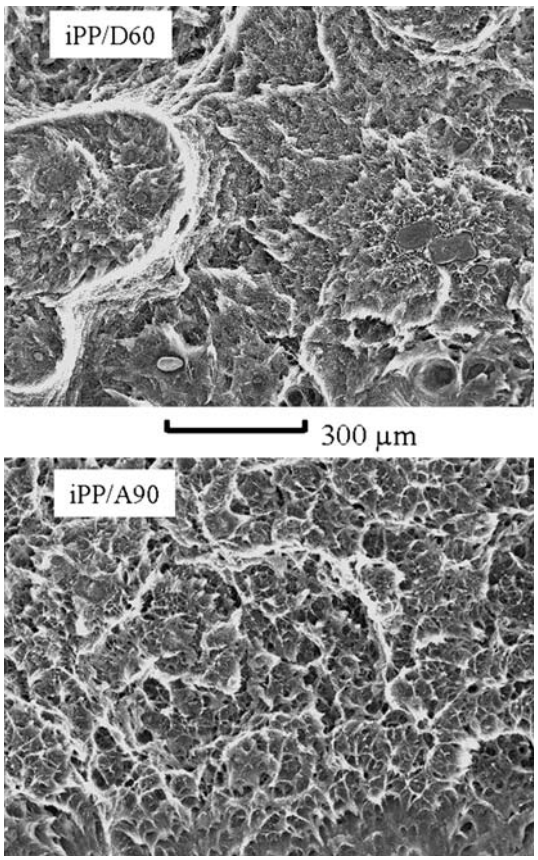

Fig. 10 SEM micrographs of tensile fracture surfaces of iPP/D60 and iPP/A90 composites

matrix. No large agglomerates of nanoparticles are observed. These improvements confirm again that the well-dispersed nanoparticles can act not only as stress concentrators but also as plasticizers in matrix as reported [24].

The mechanical properties of semicrystalline polymers are strongly affected by crystallinity and spherulite size of matrices. It is reported that an increase in crystallinity and spherulite size increases the Young's modulus and the strength of iPP, because large spherulites are believed to have a much higher load-bearing capability [25, 26]. In our study, the crystallinity degree of polymer matrix in composites increases due to nucleation effect of particles. The degree rises from 44.0% in neat iPP to 52.8% in iPP/D60 composite and to 46.9% in iPP/A90 nanocomposite. This should be the reason for that the iPP/D60 composite has higher tensile modulus by 24% whereas the iPP/A90 composite shows a comparable value as neat iPP matrix.

Conclusion

In this study, the iPP composites containing 5 wt% micro and nanoparticles were twice extruded in a Berstorff extruder. The nanoparticles are well dispersed in the matrix whereas the microparticles show a broad size distribution, which strongly affects the mechanical properties of iPP/microparticle composite. The results of mechanical characterization show that the incorporation of nanoparticles in iPP significantly increases the unnotched Charpy impact strength by 14%. The improvements in tensile stress and elongation at yield are 9 and 12%, respectively. The microparticle-filled iPP composite exhibits higher tensile modulus and yield strength than neat iPP, but much lower tensile strain and unnotched Charpy impact strength.

Acknowledgement The authors gratefully acknowledge German Research Foundation (DFG) for the fellowship in the framework of the graduate school GRK 814.

References

1. Zhou HJ, Rong MZ, Zhang MQ, Ruan WH, Friedrich K (2007) Polym Eng Sci 47:499
2. Liang JZ (2009) Polym Eng Sci 49:1603
3. Sarkar M, Dana K, Ghatak S, Banerjee A (2008) Bull Mater Sci 31:23
4. Garcia M, Van Vliet G, Jain S, Schrauwen BAG, Sarkissov A, Van Zyl WE, Boukamp B (2004) Rev Adv Mater Sci 6:169
5. Streller RC, Thomann R, Torno O, Mülhaupt R (2008) Macromol Mater Eng 293:218
6. Rong MZ, Zhang MQ, Pan SL, Friedrich K (2004) J Appl Polym Sci 92:1771
7. Velasco JI, De Saja JA, Martinez AB (1997) Fatigue Fract Eng Mater Struct 20:659
8. Chan CM, Wu JS, Li JX, Cheung YK (2002) Polymer 43:2981
9. Thio YS, Argon AS, Cohen RE, Weinberg M (2002) Polymer 43:3661
10. Huang L, Zhan RB, Lu YF (2006) J Reinf Plast Comp 25:1001
11. Lin Y, Chen HB, Chan CM, Wu JS (2008) Marcromolecules 41:9204
12. Gensler R, Plummer CJG, Grein C, Kausch HH (2000) Polymer 41:3809
13. Jancar J, Dibenedetto T (1995) J Mater Sci 30:2438. doi:10.1007/BF01184598
14. Wang G, Chen XY, Huang R, Zhang L (2002) J Mater Sci Lett 21:985
15. Lang FF, Radford KC (1971) J Mater Sci 6:1197. doi:10.1007/BF00550091
16. Rothon R (1995) Particulate-filled polymer composites. Longman, New York
17. Nielsen LE, Landel RF (1994) Mechanical properties of polymers and composites, 2nd edn. Marcel Dekker, New York
18. Lee J, Yee AF (2001) Polymer 42:577
19. Lee J, Yee AF (2001) Polymer 42:589
20. Jancar J (1999) In: Karian HG (ed) Handbook of polypropylene, polypropylene composites. Marcel Dekker, New York, Basel
21. Bartczak Z, Argon AS, Cohen RE, Weinberg M (1999) Polymer 40:2347
22. Yang JL, Zhang Z, Zhang H (2005) Compos Sci Technol 65:2374
23. Zhang H, Zhang Z, Yang JL, Friedrich K (2006) Polymer 47:679
24. Ahn SH, Kim SH, Lee SG (2004) J Appl Polym Sci 94:812
25. Ouederni M, Philips PJ (1996) J Eng Appl Sci 2:2312
26. Friedrich K (1983) Adv Polym Sci 52/53:225